$LiMn_{2-x}Ti_xO_4$ spinel-type compounds ($x \leq 1$) : structural, electrical and magnetic properties

N. Krins [a,*], F. Hatert [b], K. Traina [a], L. Dusoulier [a], I. Molenberg [c], J.F. Fagnard [c], Ph. Vanderbemden [c], A. Rulmont [a], R. Cloots [a], B. Vertruyen [a]

[a] SUPRATECS / LCIS, Chemistry Institute B6, Sart Tilman, University of Liège, B-4000 Liège, Belgium
[b] Laboratory of Mineralogy, Geology Institute B18, University of Liège, B-4000 Liège, Belgium
[c] SUPRATECS, Montefiore Institute B28, Sart Tilman, University of Liège, B-4000 Liège, Belgium

Keywords: Ti-doped $LiMn_2O_4$, Crystal structure, Magnetic properties, Impedance spectroscopy, Charge – Discharge test

Abstract

$LiMn_{2-x}Ti_xO_4$ compounds with $0 \leq x \leq 1$ were prepared by solid state reaction and Pechini technique. Powder X-ray diffraction showed that all samples crystallize with the spinel crystal structure (S.G. $Fd\bar{3}m$). The cubic unit-cell parameter increases with Ti content. The influence of the Ti content and cationic distribution on the magnetic properties of the compounds was studied by measuring the temperature and magnetic field dependences of the magnetization : substitution by non magnetic d^0 Ti^{4+} ions appeared to weaken the magnetic interactions between manganese ions. The electrical properties of $LiMnTiO_4$ were studied by AC impedance spectroscopy and DC polarisation measurements, which revealed the electronic character of the conduction process.

* corresponding author :

e-mail : nkrins@ulg.ac.be, phone : + 32 4 3663586, fax : + 32 4 3663413

1. Introduction

The normal spinel-type compound $LiMn^{3+}Mn^{4+}O_4$ presents mixed conductivity : ionic conductivity is ensured by diffusion of Li^+ ions through the channels formed by the connected vacant sites of the three-dimensional structure, while electronic conductivity results from hopping of electrons between Mn^{3+} and Mn^{4+} occupied crystallographic sites [1]. This compound has recently attracted much interest due to its potential application as a cathode material for solid state batteries [2]. However its capacity loss during cycling has up to now hindered the development of practical applications [3]. Various substitutions of manganese by other transition metal cations have been investigated in order to improve or modify the electrochemical behaviour [4, 5, 6].

In the present study, we report our results about the $LiMn_{2-x}Ti_xO_4$ solid solution (with $0 \leq x \leq 1$). Progressive substitution of Mn^{4+} cations by non magnetic d^0 Ti^{4+} ions might improve the understanding of the physical mechanisms that govern the interactions between manganese ions in $LiMn_2O_4$-type compounds. Most previous results published in the literature by other groups concerned (i) the $x \leq 0.2$ range only [7, 8] or (ii) the use of a very specific technique applied to only one defined chemical composition (EXAFS for $LiMn_{1.5}Ti_{0.5}O_4$ [9], EELS for $LiMnTiO_4$ [10], XPS for $LiMnTiO_4$ [11]). More recently, a publication by Arillo et al. [12] reported a thorough study of the $LiMnTiO_4$ compound by X-ray and neutron diffractions, magnetic and transport measurements. The originality of this work lies in the fact that we report results for the whole solid solution up to $x = 1$. We also compare the electrical transport properties of samples prepared by two different methods, displaying different microstructures, pointing out the role played by the microstructure on the physical properties.

While writing the present paper, we have become aware of a recent publication by Petrov et al. [13]: in that paper, the authors put forward a new structural model with partial

occupancy of the 8*a* crystallographic site by Mn^{2+} instead of Ti^{4+}. That issue will be further discussed in the "results and discussion" section.

The present paper is organised as follows. The synthesis of $LiMn_{2-x}Ti_xO_4$ samples (where $0 \leq x \leq 1$) by solid state reaction and Pechini technique is described in the experimental section. The "results and discussion" section is subdivided in three parts, respectively devoted to (i) the crystallographic characterisation, (ii) the dependence of the magnetic properties as a function of Ti content and (iii) the comparison of the AC and DC transport properties of $LiMnTiO_4$ samples prepared by the two synthesis methods.

2. Experimental

$LiMn_{2-x}Ti_xO_4$ samples (with $0 \leq x \leq 1$) were prepared by the conventional solid state method. Stoichiometric mixtures of lithium carbonate, manganese acetate and titanium hydroxide (prepared by hydrolysis of titanium isopropoxide) were ground in an agate mortar with petroleum ether and were heated to 623K during 1 h. The resulting powders were ground again and pressed into pellets by isostatic pressing under 2100 bar. The pellets were sintered during 24 h in air, at 1073 K for the samples with x = 0 and 0.25, and at 1223K for the samples with x = 0.5, 0.75 and 1.

A $LiMnTiO_4$ sample was also prepared by a precursor method (Pechini method [2]), in order to investigate the influence of the microstructure on the conductivity measurements. Titanium isopropoxide, manganese acetate and lithium carbonate were dissolved in ethylene glycol. Addition of citric acid led to the formation of a gel, which was dried at 493 K. The precursor was calcined at 623 K during 8 h, pelletized and sintered at 1223 K during 24 h.

X-ray powder diffraction patterns were collected using a Philips PW-3710 diffractometer with FeK_α (λ = 1.9373 Å) radiation. The scans were performed between 2θ=20° and 2θ=150° with a step size of 0.020° and a counting time of 8s/step. The structure refinement was carried out by Rietveld analysis using the DBWS-9807 program [14]. The microstructural properties

were characterized by scanning electron microscopy (Philips XL30 ESEM). The Mn/Ti ratio was measured by Energy Dispersive X-ray analysis (EDAX system coupled to the electron microscope). The lithium loss resulting from the thermal treatment was determined by atomic absorption spectrometry measurements.

The DC magnetic moment was measured as a function of temperature and magnetic field between 5 and 350 K with a Physical Property Measurement System (PPMS) from Quantum Design and a Vibrating Sample Magnetometer (VSM) from Oxford Instruments.

AC transport measurements were carried out using a Solartron 1260 Impedance Gain Phase Analyser with a frequency range of 10 Hz – 10 MHz between 298 K and 650 K. Both sides of the pellets were coated with gold in order to ensure good electrical contact with the gold blocking electrodes. Polarisation experiments in DC were performed at room temperature with a charging voltage of 1 V using a Keithley 617 Programmable Electrometer.

3. Results and discussion

3.1. Powder X-ray diffraction

Powder X-ray diffraction patterns of all samples prepared by solid state reaction could be refined in the $Fd\bar{3}m$ space group (figure 1). It turns out that the spinel structure of $LiMn_2O_4$ is retained in the substituted compounds $LiMn_{2-x}Ti_xO_4$ ($0 \leq x \leq 1$).

For $x \geq 0.5$, the ordered structural model with lithium in tetrahedral 8*a* site and manganese and titanium in the octahedral 16*d* site did not give satisfactory results. Consequently, it was necessary to introduce some disorder in the cationic distribution in order to account for the observed electron density in the 8*a* and 16*d* sites.

Previous results of X-ray and neutron diffractions for $LiMnTiO_4$ by Arillo et al. [11, 12] had shown that manganese was exclusively on the 16*d* site, while titanium was distributed in both 16*d* and 8*a* sites. Therefore a first model was used where the Mn-content of the 16*d* site was fixed to its nominal value and where Li^+ against Ti^{4+} were refined in the 8*a* and 16*d* sites.

The occupancy factors calculated from this model (Model 1) are given in Table 1. The good fit between the refined site scattering values (RSS) and the calculated site scattering values (CSS) seem to confirm this cationic distribution. However, the calculated bond valence sums (CBV) for the 8*a* crystallographic site are significantly different from the expected bond valence sums (EBV) when $0.5 \leq x \leq 1.0$ (Table 1). Because the bond valence sums are very sensitive to any change of ionic radii, they constitute a good tool to distinguish between Mn^{2+}, Mn^{3+}, Mn^{4+} and Ti^{4+} occupancy for a given crystallographic site. For this reason, the differences between the CBV and the EBV indicate that the 8*a* crystallographic site probably contains larger cations than Li^{+} and Ti^{4+}, when $0.5 \leq x \leq 1.0$.

Recently, Petrov et al. [13] proposed another model for the cationic distribution in $LiMn_{2-y}Ti_yO_4$ ($0.2 \leq y \leq 1.0$), in which Mn^{2+} shares the 8*a* position with Li, whereas Ti^{4+}, Mn^{3+}, Mn^{4+} and a small amount of Li occur in the 16*d* site. A new series of refinements was performed according to this model (Model 2), by constraining the Ti-content of the 16*d* site to its nominal value, and by refining Mn against Li in 8*a* and 16*d* sites. As shown in Table 1, the CBV are now in much better agreement with the EBV, indicating that this model is more realistic than the previous one. The unit-cell parameters and reliability factors are given in Table 2, and the final atomic coordinates, site occupancy factors, and isotropic thermal parameters are given in Table 3.

For completeness, the CBV and EBV were also calculated in the case of Mn^{3+} sharing the 8*a* position with Li, but the agreement was not better than in the case of Model 2. In conclusion our XRD refinements appear to confirm the results of Petrov et al. [13], although it contradicts the XPS results of Arillo et al. [11]. Investigation by other methods would be necessary in order to confirm the cationic distribution of model 2.

The occupancy factors obtained with models 1 and 2 (Tables 1 and 3) indicate that the main substitution mechanism involved in the $LiMn_{2-x}Ti_xO_4$ solid solution is a replacement of

Mn^{4+} by Ti^{4+} on the 16*d* site. However, in model 2, Mn^{3+} is also partially replaced by Mn^{2+} and Mn^{4+}, thus indicating a secondary substitution mechanism $2Mn^{3+}$ (16*d*) = Mn^{2+} (8*a*) + Mn^{4+} (16*d*). For x = 1.00, 0.300 Mn^{3+} per formula unit (*p.f.u.*) are replaced by 0.158 Mn^{2+} *p.f.u.* on the 8*a* site, and by 0.144 Mn^{4+} *p.f.u.* on the 16*d* site (Tables 1 and 3), thus confirming the existence of this minor substitution mechanism.

Whatever the structural model considered, the cubic unit-cell parameter (Table 2) was found to increase with titanium content (Figure 2), as could be expected considering the difference in ionic radii between Mn^{4+} ($r_{Mn4+(VI)}$= 0.530 Å) and Ti^{4+} ($r_{Ti4+(VI)}$= 0.605 Å) [15], which are the cations involved in the main substitution mechanism. As shown in Figure 2, the increase of the unit-cell parameter is not linear, probably because the secondary substitution mechanism disturbs the ideal Mn^{4+} = Ti^{4+} replacement scheme. As shown in Figure 2, the proportion of manganese in the 8*a* site, which also probably has an influence of the unit-cell parameter, does not increase linearly as a function of the substitution level.

By comparison with results from the literature [12, 13], the percentage of transition metal ions in the 8*a* site was found significantly smaller in the case of the present samples and the cubic unit-cell parameter is also smaller than in the literature for $x \geq 0.5$. This could be due to the nature of the different reactants used for the solid state synthesis : carbonate, acetate and hydroxide salts used in the present study are more reactive than commercial oxides.

Finally, it was found that the Mn/Ti ratios determined by Rietveld refinement agree well with the results deduced from EDX analysis. A lithium loss resulting from the thermal treatment was expected and thus evaluated by atomic absorption spectrometry and did not exceed 5 %.

3.2. Magnetic properties

The magnetic properties of all samples prepared by solid state reaction were measured as a function of temperature and magnetic field.

The temperature dependence of the magnetization under $\mu_0 H_{DC} = 0.1$ T was collected in Field Cooled (FC) and Zero Field Cooled (ZFC) conditions, between 5 and 350 K. Figure 3 shows the results for the samples with x = 0.25 and 0.75. For the clarity of the figure, only data in the 5K-80K range are displayed. In the case of the x = 0.25 sample, the FC and ZFC curves diverge below 40 K. The ZFC curve shows a maximum at 30 K while the FC magnetization increases down to the lowest temperature. When the Ti content is increased, the difference between the FC and ZFC curves becomes very small.

The ZFC magnetization data above 150 K could be fitted by a Curie-Weiss law $1/\chi = -\theta/C + T/C$. The inset of figure 3 shows the values of the Curie constant (C) and Weiss constant (θ) as a function of Ti content. θ is negative for all samples, which could be the signature of local antiferromagnetic exchange interactions. The absolute value of θ decreases when the Ti content is increased : this behaviour results from the weakening of the magnetic interactions between manganese ions, due to the substitution of d^0 Ti^{4+} ions in the Mn-O network.

In order to try to confirm the validity of the cationic distributions determined by Rietveld refinement, experimental values for the effective moment μ were calculated from the Curie constants and compared to the theoretical values calculated for models 1 and 2. However it was not possible to conclude because the difference between the experimental and theoretical values (typically 0.3 μ_B) is much larger than the difference between the theoretical values for the two structural models (typically less than 0.05 μ_B).

The magnetic field dependence of the magnetization was measured at 10 K and 100 K for $\mu_0 H_{DC}$ between -2 T and 2 T. The data at 10 K for the samples with x = 0.25, 0.5 and 1 are shown in figure 4. When the Ti content is increased, both the coercive field and remnant

magnetization decrease. d^0 Ti^{4+} ions do not contribute to the magnetic moment, therefore it is interesting to normalise the magnetic moment with respect to manganese content : the inset of figure 4 presents the magnetic moment of all samples in Bohr magneton per manganese ion (μ_B/Mn), for $\mu_0 H$ = 5 T, at 10 K and 100 K. The magnetic moment in μ_B/Mn increases when more titanium is substituted into the spinel structure. Indeed, when the Ti^{4+} content is increased, the average oxidation state of manganese decreases and the average number of d electrons per manganese ion increases. However the observed increase of magnetic moment is more pronounced than the linear dependence expected by this mechanism only. This confirms that Ti substitution tends to weaken the local antiferromagnetic interactions between Mn ions, as a result of the dilution of the Mn-O network by non-magnetic Ti^{4+} cations.

3.3. Electrical properties

The electrical properties of the $LiMnTiO_4$ compound were studied by AC impedance spectroscopy. In order to investigate the influence of the microstructure of the samples on the conductivity, samples prepared by two different synthesis methods were compared. Figure 5 presents electron micrographs of non-polished fractures of $LiMnTiO_4$ pellets prepared by solid state reaction (fig. 5a) or Pechini method (fig. 5b). The solid state sample is characterized by the presence of large pores and a poor connectivity between well-sintered agglomerates. On the contrary, the Pechini sample seems denser and displays better connectivity. These observations were confirmed by density measurements on the bulk pellets by Archimedes' method : the total porosity (open + closed) values obtained by this method were 18 % and 30 % for the pellets prepared by Pechini method and solid state reaction respectively.

AC impedance measurements were performed at different temperatures between 298 K and 650 K on sintered pellets of $LiMnTiO_4$ prepared by Pechini method or solid state

reaction. Figure 6 presents the complex impedance plots recorded at 298K for both samples. The impedance plot for the Pechini sample can be described as two semicircles. Assuming a series model, the semicircle at high frequency can be attributed to the intragrain conductivity while the semicircle at lower frequency is related to intergrain effects. The impedance plot for the solid state sample presents only one semicircle, whose low-frequency tail probably results from an electrode-related artefact [16]. Assuming that both samples have similar intragrain properties, the fact that only one semicircle is observed for the solid state sample suggests close values of time constants for the conductivity processes through grains and intergrain spaces. The microstructural analysis has revealed the high porosity of that sample. The geometrical capacitance associated to the large voids inside the material would be very small (0,2 pF for the solid state sample compared to 7,7 pF for the Pechini sample), which would result in a decrease of the time constant of about two orders of magnitude when compared to the Pechini sample. The significant influence of the porosity of the sample on the transport behaviour is confirmed by the higher total resistivity observed for the most porous sample (solid state sample).

The influence of the temperature on the overall conductivity is shown in figure 7, where the data for both samples are fitted by an Arrhenius equation $\sigma = A \exp(-E_a/kT)$. It turned out that the two samples present a similar activation energy, $E_a \sim 0.38$ eV. This indicates that the temperature dependence of the conductivity is probably controlled by the same activated conduction mechanism for both samples. The activation energy value does not allow to conclude about the ionic and/or electronic character of the conductivity [17] . Therefore complementary charge-discharge experiments were carried out at room temperature. Qualitatively similar results were obtained for the two samples. The data for the solid state sample are shown in the inset of figure 7. It can be seen that the total charge passed during the discharge process is ~0, revealing the predominant electronic character of the conduction

process. The resistivity values deduced from the charge process data agree well with the low frequency resistivity observed by AC impedance measurements.

4. Conclusion

$LiMn_{2-x}Ti_xO_4$ compounds with $0 \leq x \leq 1$ were prepared by solid state reaction and Pechini technique. Powder X-ray diffraction showed that all samples crystallize with the spinel-like crystal structure (S.G. $Fd\bar{3}m$). The cubic unit-cell parameter increases with Ti content. Rietveld refinements were carried out considering two different structural models, with Ti^{4+} (model 1) or Mn^{2+} (model 2) sharing the 8*a* site with Li. The best fit was obtained for model 2, despite the contradiction with previous XPS results from the literature. The magnetic properties measurements did not settle the issue and additional investigation is needed.

The influence of the Ti content on the magnetic properties of the compounds was studied by measuring the temperature and magnetic field dependences of the magnetization : substitution by non magnetic d^0 Ti^{4+} ions appeared to weaken the magnetic interactions between manganese ions. The electrical properties of $LiMnTiO_4$ were studied by AC impedance spectroscopy and DC polarisation measurements, which revealed the electronic character of the conduction process.

Acknowledgments

N.K., F.H. and B.V. thank the F.N.R.S. (National Fund for Scientific Research) in Belgium for “Research fellow” (N.K.) and “Postdoctoral researcher” (F.H. and B.V.) positions. The authors are grateful to Prof. J. Delwiche for giving us access to the VSM. Electron microscopy characterization was performed by Dr. C. Henrist from the Catμ microscopy centre. Part of this work was supported by the European Network of Excellence FAME.

Published in Solid State Ionics 177 (2006) 1033–1040

References

1. B. Ammundsen and J. Rozière, *J.Phys.Chem.* **B 101** (1997), p.8156.

2. W. Liu, G.C. Farrington, F. Chaput and B. Dunn, *J.Electrochem.Soc.* **143** (1996), p.879.

3. C. Julien, I. Mangani, S. Selladurai and M. Massot, *Solid State Sci.* **4** (2002), p.1031.

4. B. Lee, *J. Power Sources* **109** (2002), p.220.

5. Y. Sun and S. Jin, *J. Mater. Chem.* **8** (1998), p.2399.

6. B. Hwang, R. Santhanam, D. Liu and Y. Tsai, *J.Power Sources* **102** (2001), p.326.

7. K. S. Yoo, N. W. Cho and Y. Oh, *Solid State Ionics* **113-115** (1998), p.43.

8. C. Bellitto, E. Bauer, G. Righini, M. Green, W. Branford, A. Antonini and M. Pasquali, *J.Phys.Chem.Solids* **65** (2004), P.29.

9. B. Ammundsen, M. S. Islam, D. J. Jones and J.-M. Rozière, *J.Power Sources* **81-82** (1999), p.500.

10. S. Suzuki, M. Tomita, S. Okada and H. Arai, *J.Phys.Chem.Solids* **57** (1996), p.1851.

11. M. A. Arillo, M. L. Lopez, C. Pico, M. L. Veiga., A. Jimenez-Lopez and E. Rodriguez-Castellon, *J.Alloys Compd.* **317-318** (2001), p.160.

12. M. A. Arillo, G. Cuello, M. L. Lopez, P. Martin, C. Pico and M. L. Veiga, *Solid State Sci.* **7** (2005), p.25.

13. K. Petrov, R. M. Rojas, P. J. Alonso, J. M. Amarilla, M. G. Lazarraga and J. M. Rojo, *Solid State Sci.* **7** (2005), p.277.

14. R. A. Young, A. Saktivel, T. S. Moss and C. O. Paiva-Santos, *J.Appl.Cryst*. **28** (1995), p.366.

15. R. D. Shannon, *Acta Crystallogr. A* **A32** (1976), p.751.

16. J.R. Mac Donald., *Impedance Spectroscopy : Emphasizing Solid Materials and Systems*, Wiley, New-York, 1987.

17. P. Martin, M. L. Lopez, M. Veiga, and C. Pico, *Solid State Sci.* **6** (2004), p.325.

Figure captions

Fig.1. Powder X-ray diffraction pattern of the $LiMn_{1.5}Ti_{0.5}O_4$ sample prepared by solid state reaction at 1223 K. Experimental data were refined in the $Fd\bar{3}m$ space group. The difference curve between the measured and calculated data is shown at the bottom of the graph.

Fig. 2. Cubic lattice parameter and Mn percentage in 8a site as a function of titanium content.

Fig. 3. Main figure : Temperature dependence of the Field Cooled (FC) (white symbol) and Zero Field Cooled (ZFC) (black symbol) magnetization under $\mu_0 H_{DC} = 0.1$ T for the samples with x = 0.25 (triangle) and 0.75 (square) . Only one third of data points are shown on the figure. Inset : Curie (C) and Weiss (θ) constants obtained by fitting a Curie-Weiss law to the ZFC magnetization data for the samples $LiMn_{2-x}Ti_xO_4$ ($0 \leq x \leq 1$).

Fig. 4. Main figure : Field dependence of the magnetization of the samples $LiMn_{2-x}Ti_xO_4$ (with x = 0.25, 0.5, 1) at 10K. Inset : Magnetization (in μ_B/Mn) for $\mu_0 H = 5$ T, at 10 and 100K, as a function of titanium content.

Fig. 5. Electron micrographs of non-polished fractures of $LiMnTiO_4$ pellets prepared (a) by solid state reaction or (b) by Pechini method.

Fig. 6. Complex impedance plot at 298 K for $LiMnTiO_4$ synthesized by Pechini and solid state routes.

Fig. 7. Main Figure : Charge and discharge measurements for $LiMnTiO_4$ synthesized by Pechini (a) solid state (b) method. Inset: Charge and discharge measurements for $LiMnTiO_4$ obtained by solid state route

Table 1. Comparison of the two cationic distribution models, used during the powder X-ray Rietveld refinement of the $LiMn_{2-x}Ti_xO_4$ spinel-type compounds.

Model 1										
	X = 0.00		**X = 0.25**		**X = 0.50**		**X = 0.75**		**X = 1.00**	
	8a	***16d***	***8a***	***16d***	***8a***	***16d***	***8a***	***16d***	***8a***	***16d***
Li	1.000	-	1.000	-	0.944	0.020	0.884	0.044	0.828	0.080
Mn^{2+}	-	-	-	-	-	-	-	-	-	-
Mn^{3+}	-	0.500	-	0.500	-	0.524	-	0.542	-	0.500
Mn^{4+}	-	0.500	-	0.375	-	0.226	-	0.083	-	-
Ti^{4+}	-	-	-	0.125	0.056	0.230	0.116	0.331	0.172	0.420
MBL	1.980	1.954	1.978	1.961	1.990	1.964	1.996	1.970	1.995	1.980
RSS	2.82	25.43	3.18	24.96	4.06	23.87	5.20	23.04	6.27	21.98
CSS	3.00	25.00	3.00	24.63	4.06	23.87	5.20	23.04	6.27	21.98
EBV	1.00	3.50	1.00	3.50	1.17	3.42	1.35	3.33	1.52	3.26
CBV	1.00	3.52	1.00	3.53	1.02	3.51	1.07	3.44	1.13	3.31
Model 2										
	X = 0.00		**X = 0.25**		**X = 0.50**		**X = 0.75**		**X = 1.00**	
	8a	***16d***	***8a***	***16d***	***8a***	***16d***	***8a***	***16d***	***8a***	***16d***
Li	1.000	-	1.000	-	0.940	0.021	0.893	0.039	0.842	0.078
Mn^{2+}	-	-	-	-	0.060	-	0.107	-	0.158	-
Mn^{3+}	-	0.500	-	0.500	-	0.471	-	0.436	-	0.350
Mn^{4+}	-	0.500	-	0.375	-	0.259	-	0.150	-	0.072
Ti^{4+}	-	-	-	0.125	-	0.250	-	0.375	-	0.500
MBL	1.980	1.954	1.978	1.961	1.990	1.964	1.996	1.970	1.995	1.980
RSS	2.82	25.43	3.18	24.96	4.32	23.81	5.35	23.02	6.48	21.78
CSS	3.00	25.00	3.00	24.63	4.32	23.81	5.35	23.02	6.48	21.78
EBV	1.00	3.50	1.00	3.50	1.06	3.47	1.11	3.45	1.16	3.42
CBV	1.00	3.52	1.00	3.53	1.02	3.53	1.05	3.48	1.10	3.35

MBL = mean bond lengths (Å; the estimated standard deviations on these values are estimated to be ca. 0.002 Å), RSS = refined site scattering values (electrons per formula unit), CSS = calculated site scattering values (electrons per formula unit), EBV = expected bond valence sums (valence units), CBV = calculated bond valence sums (valence units). The total occupancies of each crystallographic site has been constrained to 1.000. The CBV have been calculated with the empirical parameters of Brown & Altermatt (1985), and the EBV have been calculated by multiplying the site occupancies by the charges of the corresponding cations on a crystallographic site.

Table 2. Unit-cell parameters and reliability factors for the $LiMn_{2-x}Ti_xO_4$ spinel-type compounds (S.G. $Fd\bar{3}m$). The forms of the reliability factors are given by Young et al. (1998).

	X = 0.00	**X = 0.25**	**X = 0.50**	**X = 0.75**	**X = 1.00**
R_p (%)	2.74	2.56	2.24	2.56	2.86
R_{wp} (%)	4.60	4.20	3.24	3.42	3.80
$R_{exp.}$ (%)	1.61	1.77	2.04	2.24	2.55
S	2.86	2.36	1.58	1.52	1.49
R_{Braqg} (%)	7.06	4.84	4.06	5.30	5.78
a (Å)	8.243(1)	8.257(1)	8.282(1)	8.308(1)	8.334(1)

Table 3. Positional (*x*, *y*, *z*), isotropic thermal (*B*) and site occupancy (*N*) parameters for the $LiMn_{2-x}Ti_xO_4$ spinel-type compounds.

Atom	Wyckoff	*x*	*y*	*z*	*B* (Å^2)	N
$LiMn_2O_4$ (x = 0.00)						
Li	8*a*	0.125	0.125	0.125	0.3(4)	0.94(3)
Mn	16*d*	0.50	0.50	0.50	1.17(4)	1.017(9)
O	32*e*	0.2637(2)	0.2637(2)	0.2637(2)	1.6(1)	1.00
$LiMn_{1.75}Ti_{0.25}O_4$ (x = 0.25)						
Li	8*a*	0.125	0.125	0.125	0.6(4)	1.06(3)
Mn	16*d*	0.50	0.50	0.50	1.10(4)	0.875
Ti	16*d*	0.50	0.50	0.50	1.10(4)	0.14(1)
O	32*e*	0.2633(2)	0.2633(2)	0.2633(2)	1.3(1)	1.00
$LiMn_{1.50}Ti_{0.50}O_4$ (x = 0.50)						
Li	8*a*	0.125	0.125	0.125	1.00	0.940(2)
Mn	8*a*	0.125	0.125	0.125	1.00	0.060(2)
Mn	16*d*	0.50	0.50	0.50	1.10(4)	0.73(1)
Ti	16*d*	0.50	0.50	0.50	1.10(4)	0.25
Li	16*d*	0.50	0.50	0.50	1.10(4)	0.02(1)
O	32*e*	0.2639(1)	0.2639(1)	0.2639(1)	1.3(1)	1.00
$LiMn_{1.25}Ti_{0.75}O_4$ (x = 0.75)						
Li	8*a*	0.125	0.125	0.125	0.4(3)	0.893(4)
Mn	8*a*	0.125	0.125	0.125	0.4(3)	0.107(4)
Mn	16*d*	0.50	0.50	0.50	1.43(5)	0.59(1)
Ti	16*d*	0.50	0.50	0.50	1.43(5)	0.375
Li	16*d*	0.50	0.50	0.50	1.43(5)	0.04(1)
O	32*e*	0.2637(2)	0.2637(2)	0.2637(2)	1.5(1)	1.00
$LiMnTiO_4$ (x = 1.00)						
Li	8*a*	0.125	0.125	0.125	0.4(2)	0.842(4)
Mn	8*a*	0.125	0.125	0.125	0.4(2)	0.158(4)
Mn	16*d*	0.50	0.50	0.50	1.52(5)	0.42(1)
Ti	16*d*	0.50	0.50	0.50	1.52(5)	0.50
Li	16*d*	0.50	0.50	0.50	1.52(5)	0.08(1)
O	32*e*	0.2632(2)	0.2632(2)	0.2632(2)	1.6(1)	1.00

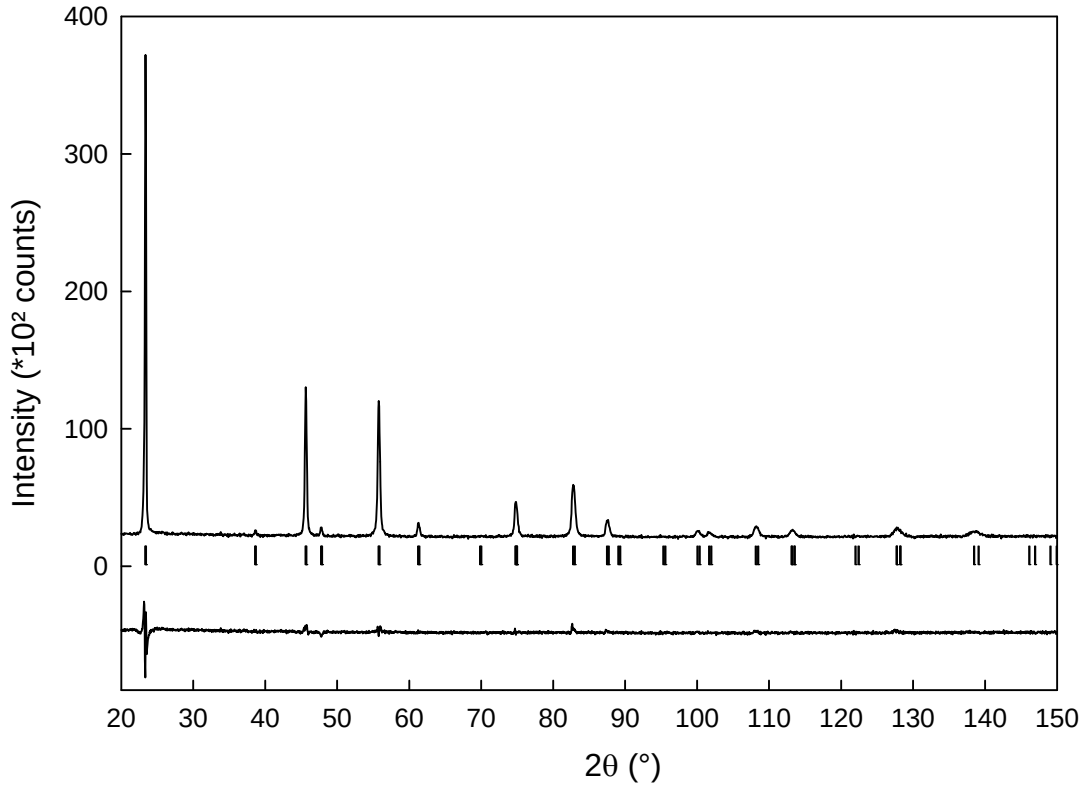
400
300
200
100
0
Intensity (*10² counts)
20
30
40
50
60
70
80
90
100
110
120
130
140
150
2θ (°)

Fig. 1

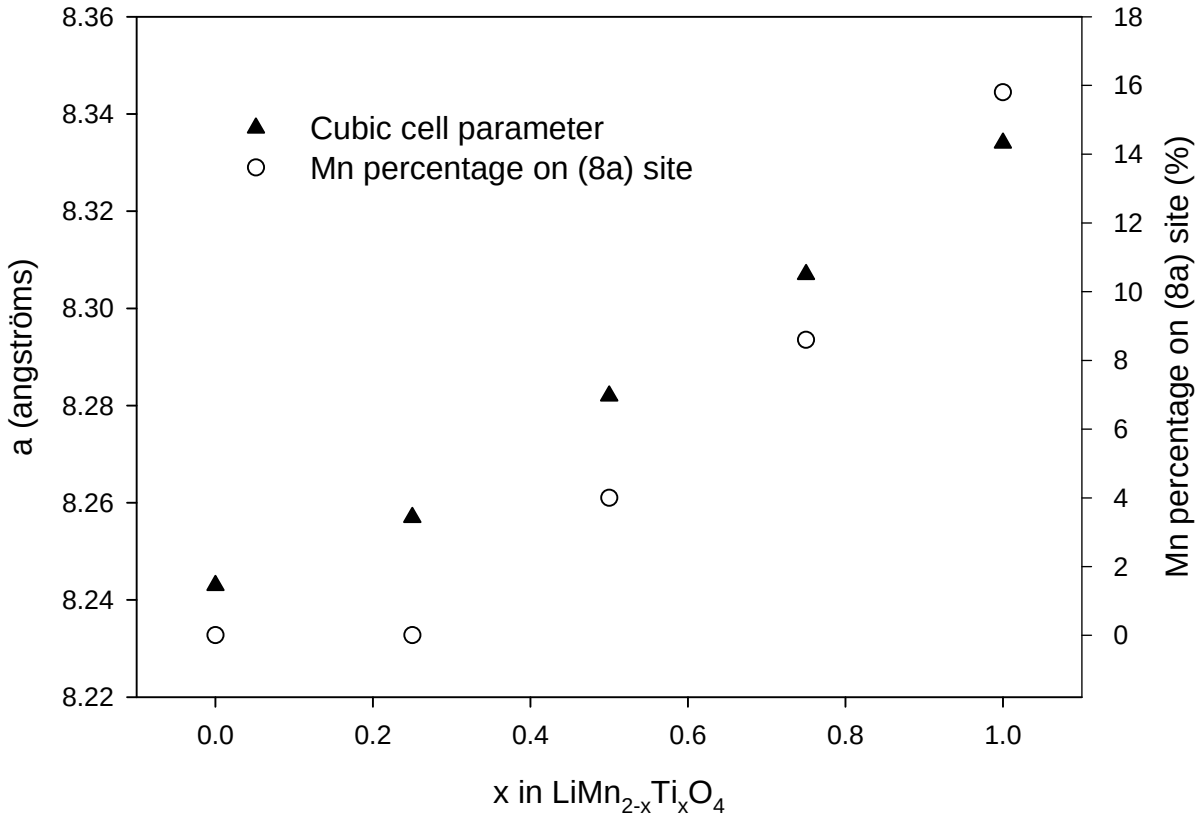
8.36
8.34
8.32
8.30
8.28
8.26
8.24
8.22
a (angströms)
18
16
14
12
10
8
6
4
2
0
Mn percentage on (8a) site (%)
Cubic cell parameter
Mn percentage on (8a) site
0.0
0.2
0.4
0.6
0.8
1.0
x in LiMn2-xTixO4

Fig. 2

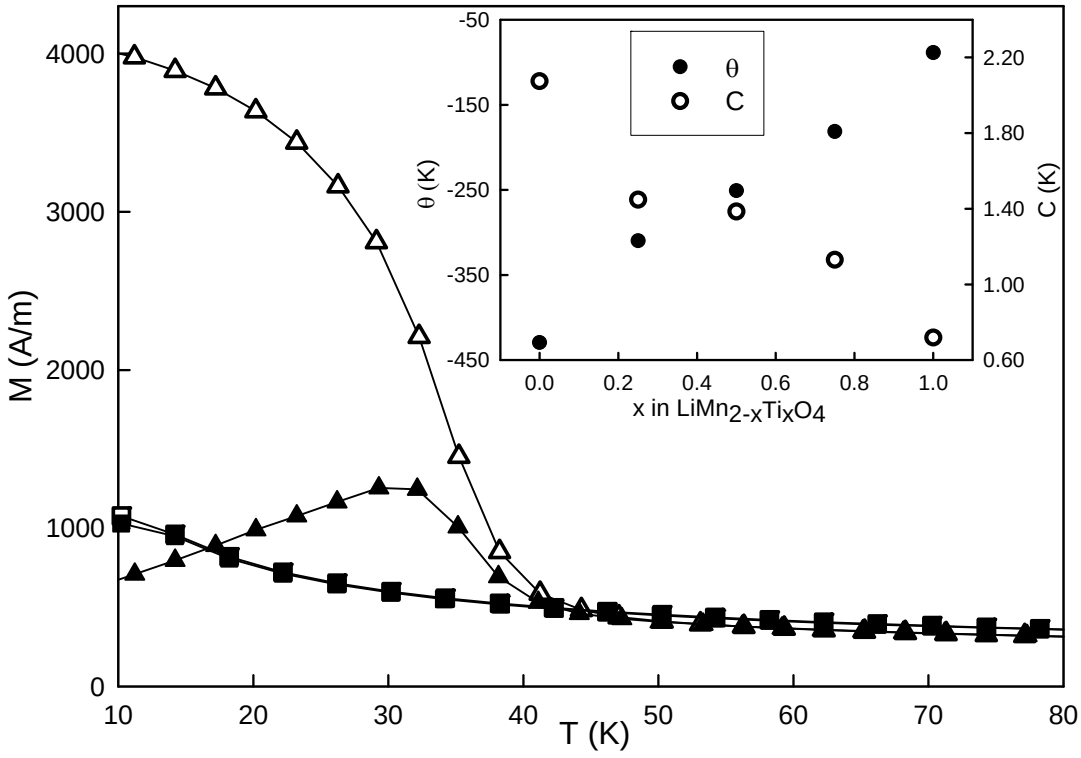

Fig. 3

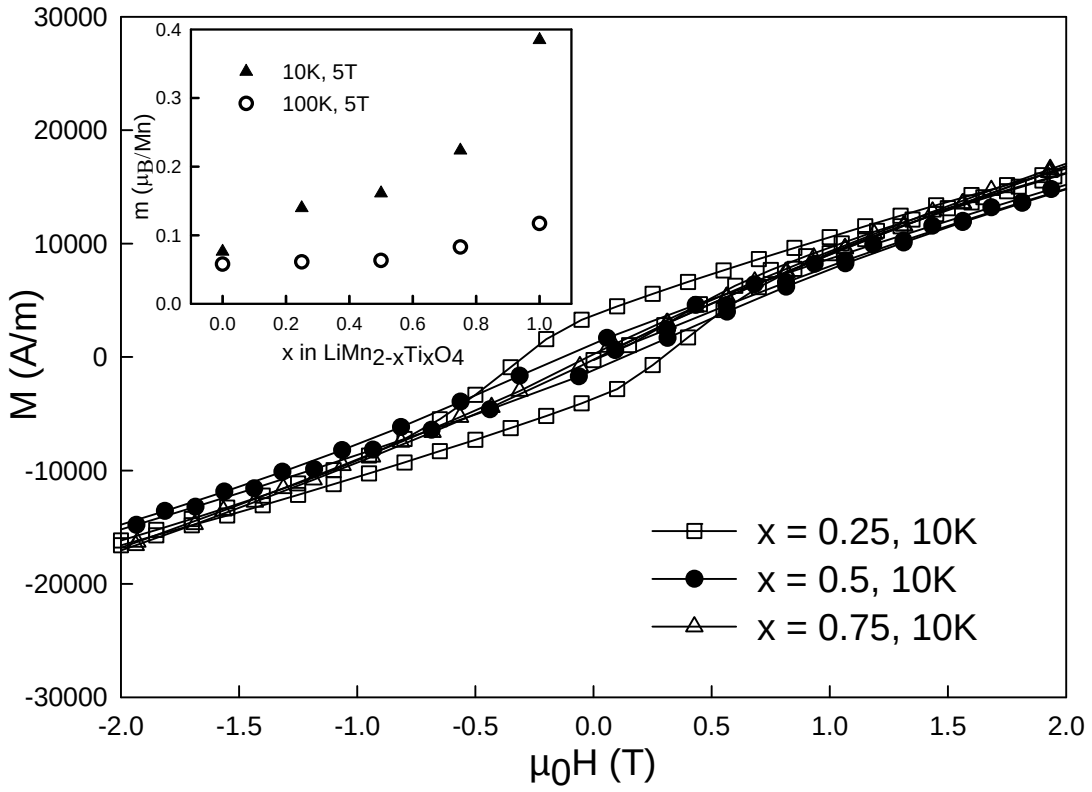
30000
20000
10000
0
-10000
-20000
-30000
M (A/m)
-2.0
-1.5
-1.0
-0.5
0.0
0.5
1.0
1.5
2.0
μ0H (T)
x = 0.25, 10K
x = 0.5, 10K
x = 0.75, 10K
0.4
0.3
0.2
0.1
0.0
m (μB/Mn)
10K, 5T
100K, 5T
0.0
0.2
0.4
0.6
0.8
1.0
x in LiMn2-xTixO4

Fig. 4

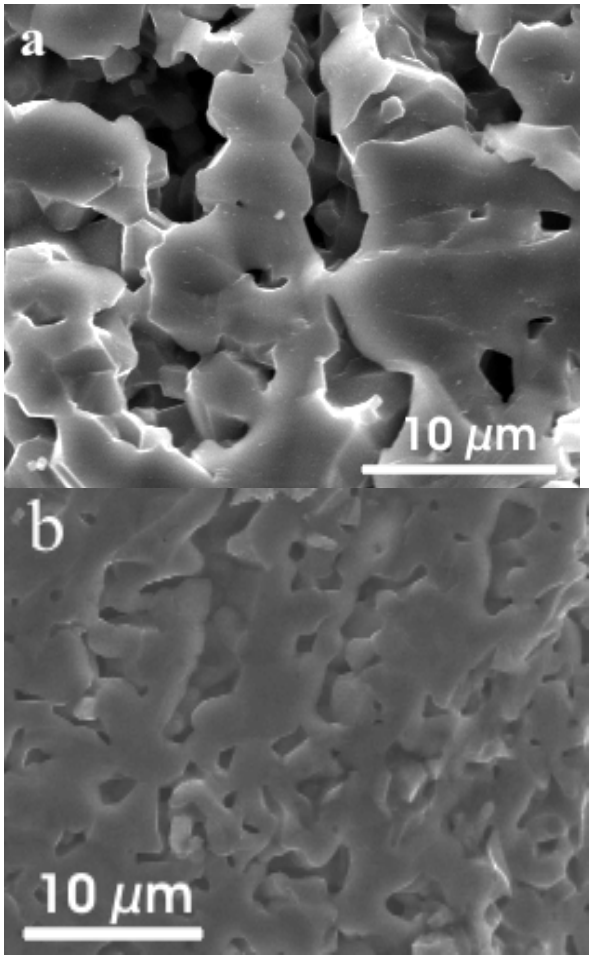

Fig. 5

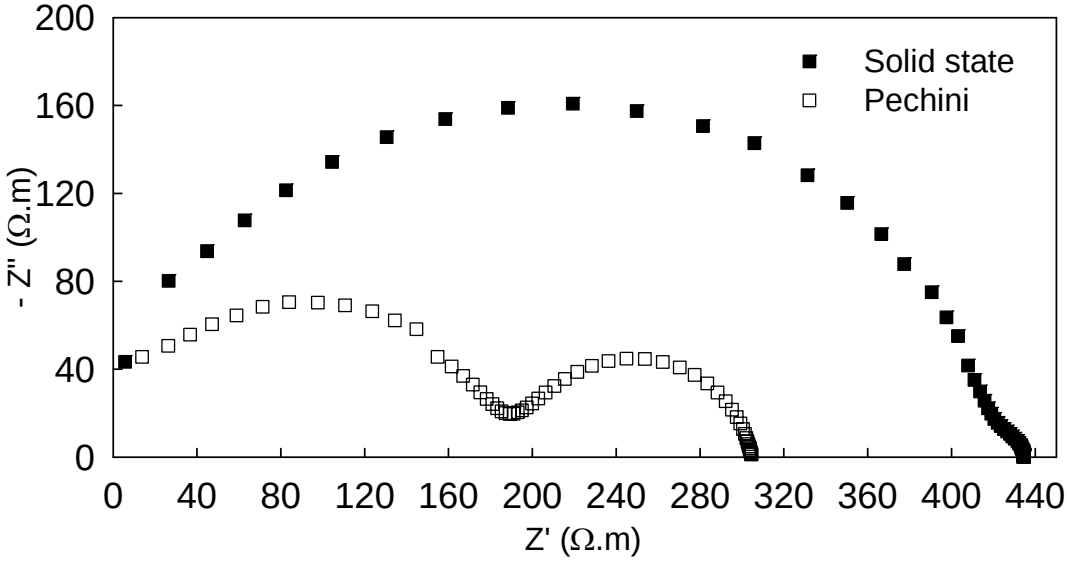
Solid state
Pechini
- Z'' (Ω.m)
Z' (Ω.m)
0
40
80
120
160
200
240
280
320
360
400
440

Fig. 6

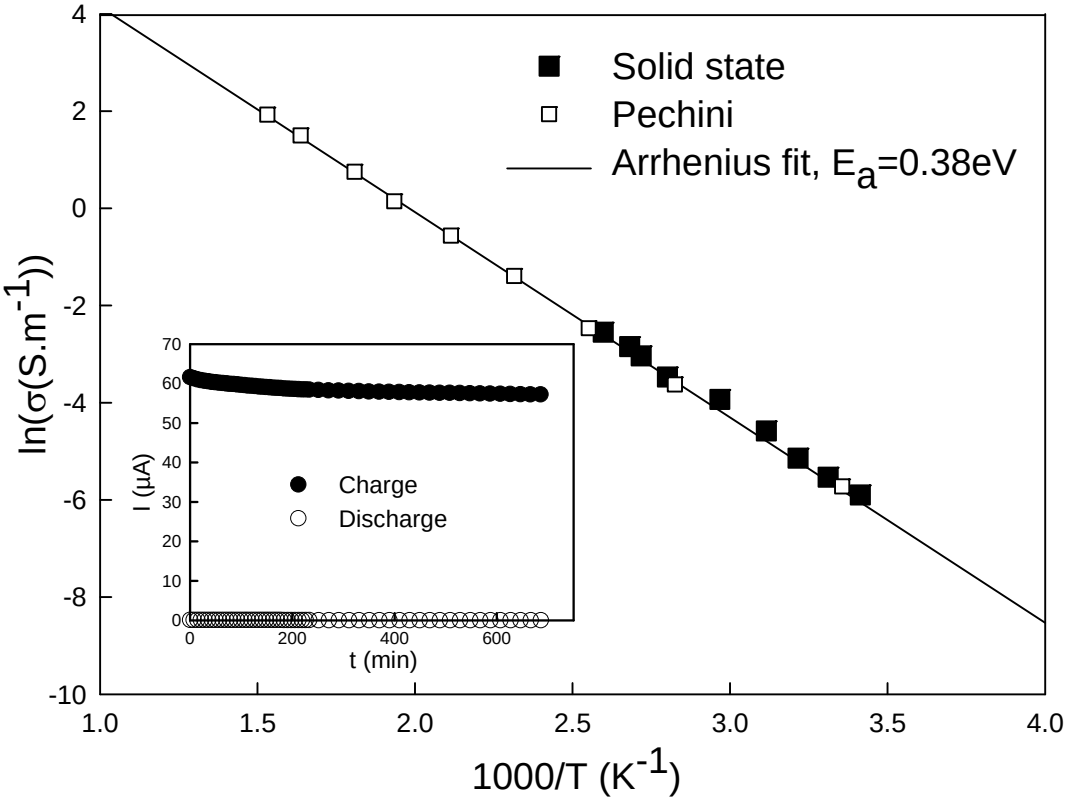
Solid state
Pechini
Arrhenius fit, E_a=0.38eV
ln(σ(S.m^{-1}))
1000/T (K^{-1})
I (μA)
t (min)
Charge
Discharge

Fig. 7